



Merensky pillar strength formulae based on back-analysis of pillar failures at Impala Platinum

by B.P. Watson*, J.A. Ryder†, M.O. Kataka*, J.S. Kuijpers*, and F.P. Leteane*.

Synopsis

The Bushveld platinum group metal deposits are two distinct, shallow-dipping stratiform tabular orebodies and strike for many hundreds of kilometres. Mining is extensive, with depths ranging from close-to-surface to 2 000 m. The mining method is a variation of planar open stope. Pillars are widely used to support the open stopes. Little work has been done in the past to determine pillar strength and pillars have been designed using experience and formulae developed for other hard-rock mines. This has led to oversize pillars with consequential loss of ore or undersize pillars resulting in potential collapses or pillar bursts. This paper describes a back-analysis of pillar failures at Impala Platinum, just north of Rustenburg, and provides insights into pillar behaviour. Strength formulae are presented for Merensky Reef pillars at Impala. These formulae may be used cautiously on other platinum mines with similar geotechnical and geomechanical conditions.

Introduction

The Bushveld Complex is a large layered igneous intrusion which spans about 350 km from east to west. It is situated in the northern part of South Africa (Figure 1). The platinum group metals are concentrated in two planar orebodies known as the Merensky Reef, a mineralized pegmatoidal pyroxenite 0.7 m to 1.4 m thick, and, underlying this, the UG2 Reef comprising one or more chromitite seams of similar thickness.

The strata generally dip at 8° to 15° toward the centre of the complex. The horizontal to vertical stress ratio (k ratio) varies from about 0.5 to over 2.5. The depth of mining ranges from outcrop to 2 300 m.

In the mining depth range from surface to about 1 400 m, the vertical tensile zone often extends high into the hangingwall. If a sufficiently large mining span is achieved, or the stope abuts a geological feature, a large volume of hangingwall rock can become unstable, resulting in a stope collapse, or colloquially, a 'backbreak'¹. In order to prevent these backbreaks a high resistance support system is required. This is universally achieved by the use of small in-stope chain pillars orientated either on strike for breast

mining (Figure 2) or on dip for up-or down-dip mining.

In the past, pillar design on the Merensky and UG2 reefs has been done using experience and strength formulae derived for other hard-rock mines. The consequence of this uncertain methodology is to cut oversize pillars, which lowers the extraction ratio. In addition, pillars cut in the deeper levels are required to fail in a stable manner soon after being cut. These pillars are known as crush pillars and their residual strengths provide the required support resistance to prevent backbreaks and keep the stope hangingwall stable. A recent series of pillar bursts, with serious consequences, has raised questions about the design of these pillars. A maximum likelihood back-analysis study was conducted on failed and stable pillars, and strength formulae were developed for the Merensky Reef at Impala Platinum (just north of Rustenburg, Figure 1).

Data collection procedures

Site observations

The *in situ* dimensions of the evaluated pillars were directly measured and the presence/absence of sidings adjacent to pillars was noted. Pillar condition was documented according to the following scale of condition codes (CC):

- 5: Pillar heavily damaged, date/geometry at failure not accurately known
- 4: Pillar presumed failed, date/geometry at failure not accurately known

* CSIR, Johannesburg, Gauteng, South Africa

† Ryder Marketing and Research, Johannesburg, Gauteng, South Africa

© The Southern African Institute of Mining and Metallurgy, 2008. SA ISSN 0038-223X/3.00 + 0.00. This paper was first published at the SAIMM Symposium, Ground Support in Mining and Civil Engineering Construction, 30 March–3 April 2008.

Merensky pillar strength formulae based on back-analysis of pillar failures

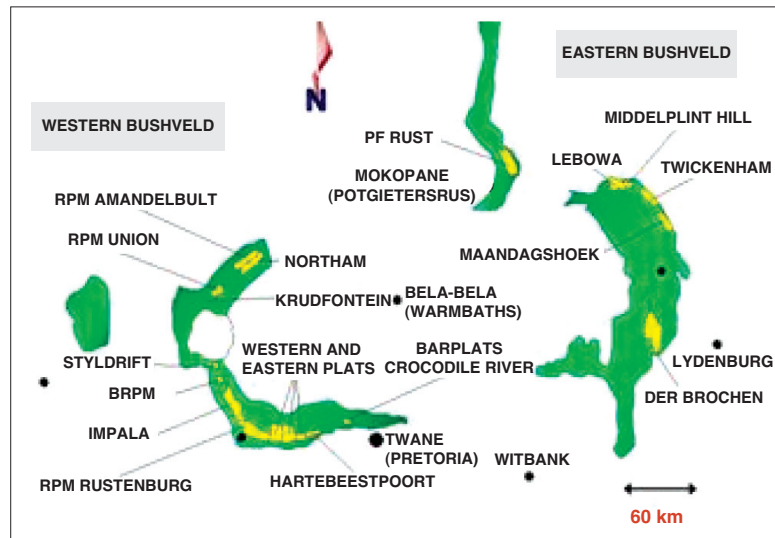


Figure 1—The extent of the Bushveld platinum exposure

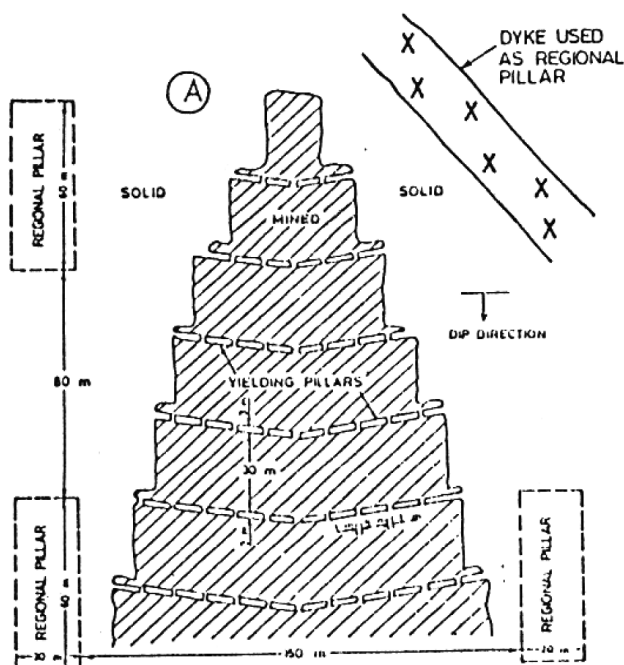


Figure 2—Plan view of a typical stope on one of the platinum orebodies

- 3: Pillar definitely failed (or burst), date/geometry at failure known
- 2: Pillar sidewalls visibly fractured/scaled, date/geometry known
- 1: Pillar sidewall scaling barely visible, date/geometry known
- 0: Pillar with no visible damage, date/geometry known.

Pillars with condition code 3 are the most directly relevant for back-analysing strength parameters, although pillars with other codes give confirmatory information.

Pillar load estimation

Pillar loads were estimated using pseudo 3D, elastic, MinSim²

and MINF³ modelling. Mine plans were digitized, capturing in each instance an area large enough to provide realistic stress conditions. Usually, these conditions were inferred by direct modelling and subsequent elimination of superfluous abutting mining windows. In many cases, it was necessary to estimate a 'correction factor' (CF), based on a comparison of coarse-grid average pillar stress (APS) values on large pillars near the areas of interest, with and without a large flanking area of mining. Such factors were generally less than 1.2 (20% correction), and were, where feasible, checked using Equation [1]⁴. This equation may be used if there is a large sea of mining with roughly uniform convergence S over a sector θ bounded by radii R_1 and R_2 (Figure 3).

$$\left(\frac{\sigma_{zz}}{q}\right) \approx S \left(\frac{\theta}{2\pi}\right) \left(\frac{1}{R_1} - \frac{1}{R_2}\right) \quad [1]$$

Sector of mining,
angle = θ
arcs at R_1 R_2

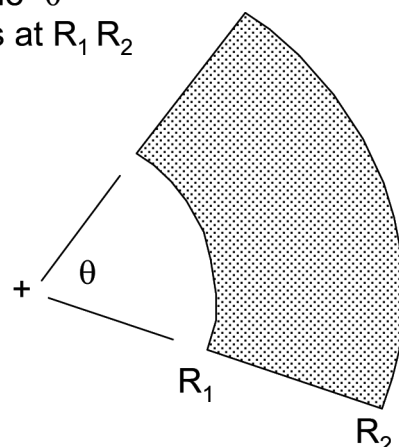


Figure 3—Areas of remote mining, well outside the centre (+) of the area of interest

Merensky pillar strength formulae based on back-analysis of pillar failures

$\bar{S} = (E^*S/q)$ is the normalized average convergence in this region, where S is the convergence and q is the virgin vertical stress. $E^* = E/4(1-\nu^2)$ where E is the Young's modulus and ν is the Poisson's ratio.

If, for example, the RHS of Equation 1 evaluates to 0.002, then the driving stress on the area of interest, and all calculated convergence or APS values, need to be increased by 0.2 %.

A grid size of 0.5 m was used in order adequately to capture true pillar dimensions in the area of interest. The modelling results were validated, where possible, by analytic solutions and by comparing MinSim and MINF results. Errors of less than 10% in APS values are estimated from the numerical modelling.

Generally a series of runs was carried out. In the first run, all small pillars were modelled as intact structures. In the second run, any pillars carrying more load and being smaller than known failed pillars in an area of interest were deemed to have failed, assigned a CC of 4 or 5, and allocated a residual stress of 20 MPa as suggested by Watson *et al.*⁵ and Roberts *et al.*⁶. This procedure was repeated until no further pillars fulfilled the failure criterion.

In the analysis, pillar height has been corrected to allow for the presence of gullies unprotected by sidings using Equation [2]. The correction is based on numerical modelling performed by Roberts *et al.*⁷.

$$h_e \approx [1 + 0.2692(w/h)^{0.08}] h \quad [2]$$

where w and h are the pillar width and mining height respectively.

As a typical example, the effective height (in terms of expected strength) of a sidingless pillar with a gully depth of 2.0 m increases from 1.2 m to about 1.6 m.

Pillar effective widths (w_e) account for rectangular pillars, taking cognisance of pillar length (L) according to the widely used 'perimeter rule', described by Wagner⁸:

$$w_e \approx 2 w L / (w + L) \quad [3]$$

Strength parameter estimation

The strength of a pillar may be assumed to be a function of its known physical characteristics (including width, height, length), and certain unknown parameters (e.g. Salamon and Munro⁹ K , α , β values). The maximum likelihood analysis was used to estimate a best fit for these parameters. (This type of statistical back-analysis accounts for the many variables that contribute to pillar strength without necessarily needing to understand the failure mechanisms.) The process involved the evaluation of a database of APS values calculated by MinSim where the 'condition', i.e. 'intact' or 'failed', was known.

Following the approach of Salamon and Munro⁹, the safety factor (SF) of each pillar was defined by:

$$SF = \text{Strength} / \text{APS} \quad [4]$$

A probabilistic distribution of SFs governs the condition of pillars, in the sense that a pillar with $SF > 1$ is likely to be intact, while one with $SF < 1$ is likely to have failed. A lognormal distribution was assumed for the SFs, having a log-mean of zero and standard deviation of s . With this formulation, physically meaningless negative SFs are disbarred, and reciprocal symmetry pertains, e.g. a pillar having $SF = 0.5$ is about as likely to have failed as one with $SF = 2$ to have not failed. The logarithmic standard deviation

was assumed to account for all uncertainties in the system of pillars, e.g. mismeasurement of widths, misestimation of pillar APS values, real geotechnical variations in pillar properties, etc. For historical reasons, logarithms to base 10 are used in the lognormal distribution, and to interpret s , $10^{\pm s}$ needs to be evaluated in relation to unity. The value of s is a parameter that has to be estimated along with the unknown parameters governing the strength of the pillars in a given observed set.

A 'likelihood function' (L_i) of the probability of the pillars exhibiting their stipulated condition ('intact' or 'failed') was set up. To avoid multiplications, the logarithm (base e) of L_i was used so that the function F was defined as in Equation [5]:

$$F = \ln L_i = \sum \ln(\text{prob. of intact cases}) + \sum \ln(\text{prob. of failed cases}) \quad [5]$$

The probability of an intact case (condition codes CC = 0, 1, or 2 in this study) was given by $\Phi(\log SF)$ where Φ is the cumulative normal distribution. Such cases biased the derived best parameter fits so that their SFs were as large as possible.

The probability of a failed case in which the APS value was the estimated load at which failure actually occurred (the situation in Salamon and Munro's⁹ back analysis, and CC=3 in the present study) was given by $\Phi(\log SF)/SF$, where Φ is the normal probability density function. These cases strongly biased the best-fit parameters so that their SFs were more or less symmetrically disposed about unity. Note that this corresponds exactly to the formulation presented in Salamon and Munro⁹.

The probability of a failed case where the APS was merely an upper bound and failure probably took place earlier at some lower APS value (the situation in many of the back-analysis scenarios, CC = 4 or 5) was expressed by the function $(1 - \Phi(\log SF))$. This is analogous to the treatment of intact cases, and biased the best-fit parameters so that the SFs were as small as possible. The fit is weaker than for the situation where APS values reflect actual strengths at which failure occurred.

Validation of the numerical models used to determine pillar strength

A system of regularly spaced, stable, rib pillars at Lonmin Karee provided an unusual quasi-2D situation where the numerical models could be validated against an analytic solution. Figure 4 depicts the geometry of this site.

A 7 m wide by 1.4 m high dip pillar, with 28 m mined-out panels on either side, was observed *in situ* to be just beginning to scale (CC=1). The APS provided by the MinSim model was 80.8 MPa. This result compared favourably with an analytic estimate of 82 MPa. The area of interest was about 660 m below surface.

Data collection sites

Introduction

A total of five stopes from three shafts at Impala were used in the evaluation. The pillars were composite, consisting of pyroxenite and anorthosite with a 1 cm wide chromitite stringer at the pillar centre (Figure 5). Generally the pillars consisted of equal parts of pyroxenite and anorthosite.

Merensky pillar strength formulae based on back-analysis of pillar failures

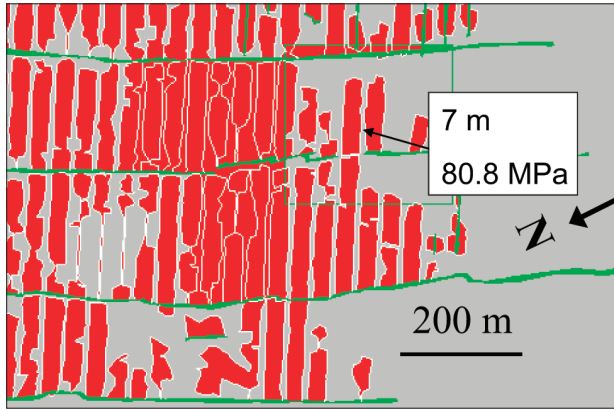


Figure 4—Karee dip pillar geometry (grid size 0.5 m, depth 660 m, dip 9°, slope width 1.4 m, $k = 1$)

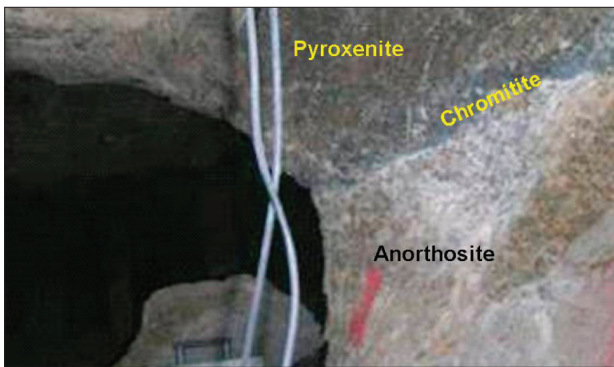


Figure 5—A typical composite pillar used in the statistical evaluations

Pyroxenite and anorthosite samples were collected from one of the investigated pillars and tested in a stiff-testing machine. Figure 6 and Figure 7 show the stress-strain behaviour of these rock types under uniaxial and triaxial testing conditions.

The geomechanical behaviours of the two rock types differ slightly from one another, which would have resulted in complex interactions during loading. The more brittle Type II behaviour¹⁰ shown by the anorthosite in Figure 7 could explain why some pillars burst, while others of similar size do not, i.e. pillars with a higher proportion of anorthosite may be more vulnerable to bursting.

Impala 4 shaft

In 1968 Impala Platinum introduced a system of nominal 5 m by 5 m pillars, spaced 32 m by 30 m (centre-to-centre). The system supported the stopes until August 1974, when a massive collapse involving an area of roughly 200 m by 200 m in a recently holed pair of stopes (total strike span of 600 m) occurred at a depth of 160 m (Figure 8). The hangingwall failure affected surface structures, including the mine hospital. The fall was bounded on the up- and down-dip extremities by a fault and dyke respectively. No potholes were present in the stope and the extraction ratio was about 98%. Pillar loads, based on tributary area theory, were estimated at about 240 MPa¹¹, and the suggested mechanism

of failure was the activation of the bounding weak planes, which removed the bridging effect of the strata and applied full overburden loads to the pillars. Pillars appeared heavily damaged, but no loss of integrity of hangingwall or pillar foundations was seen. Since this is one of the few well-documented hard-rock collapse scenarios in South Africa, it was included in this study.

The pillars reported as the worst affected were selected for the strength analyses and are highlighted by the dotted block in Figure 8. This area also formed part of the highest elastic convergence in the evaluation and therefore the most vulnerable region between the fault and dyke structures (see the dotted region between the geological structures in Figure 8). Closure was estimated from underground visits

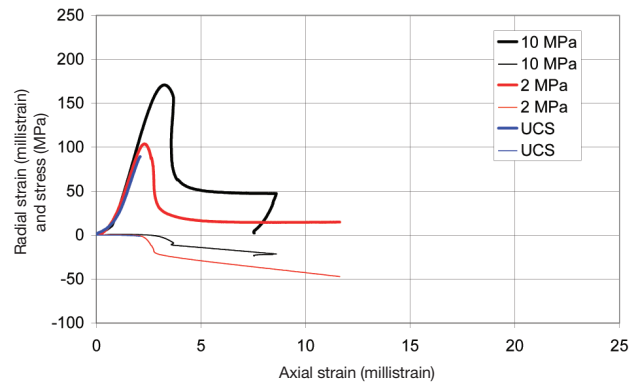


Figure 6—The stress-strain behaviour of the pyroxenite rock type

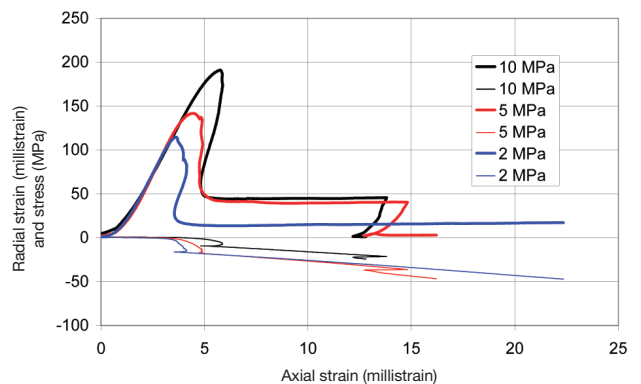


Figure 7—The stress-strain behaviour of the anorthosite rock type

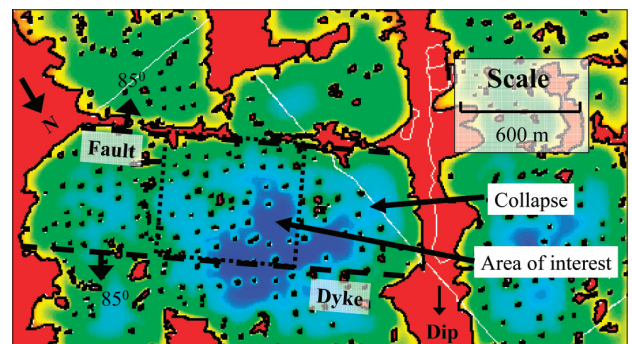


Figure 8—Impala 4 shaft collapse site (depth 160 m, dip 9°)

Merensky pillar strength formulae based on back-analysis of pillar failures

just after the collapse to be about 300 mm in the area of interest and varied between 40 mm and 150 mm over the rest of the collapse. Surface deformations above the worst affected area were also 300 mm, suggesting that the block slipped down on the fault and dyke structures with very little bulking. Further justification for the participation of the fault and dyke in the collapse was provided when cracks matching the extrapolated positions of the underground structures were observed on surface.

The modelling of this site was particularly difficult, since not only was there extensive remote mining, but, at a mean depth of only 160 m, the finite depth effect had to be taken into account. This was accomplished by assuming a second, completely mined out reef, on surface elevation, about four times larger than the area of interest. The effects of remote mining were included by modelling a basic window size of 1 024 m by 1 024 m to establish a correction factor. After this the area of interest (256 m by 256 m) was modelled using a grid size of 0.5 m and the results corrected for external mining using a factor of 1.26.

Further analysis of the MinSim finite-depth run revealed that the stress carried by all pillars in the collapse area, averaged over this area, amounted to 3.5 MPa. If the mechanism of preliminary rupture of the bounding dyke/fault structures is correct, the average would be 4.8 MPa, i.e. cover load tributary area. This is about 37% higher than the MinSim evaluation. Since the stresses shown by the MinSim analysis were already very high, a more likely mechanism is that one or two pillars failed at about 180 MPa (the elastic stress calculated by MinSim for the smallest pillars), triggering a pillar run and the final general collapse, along with failure of the bounding dyke/fault structures. The pillar with the highest stress was also the smallest pillar. It was therefore assigned CC3 and included in the database.

Impala 8 shaft

During the mid-1990s, Impala Platinum returned to some old, shallow-depth Merensky workings to mine out the in-stope pillars between barrier pillars spaced 140 m to 200 m apart. The investigated stope is located about 320 m below surface and is shown in Figure 9. An area of about 140 m x

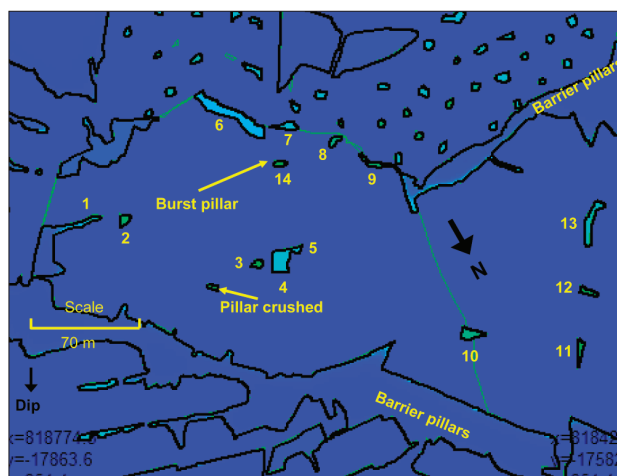


Figure 9—Plan showing the Impala 8 shaft investigation site (depth 320 m, dip 9°)

300 m is isolated from the surrounding stopes by significant pillars on all four sides. The only pillars left within the area of interest are shown in Figure 9.

Pillar 14 burst some time after the in-stope pillars were extracted from the original stope (Figure 10). The stress carried by the pillar at the time of failure was calculated using MinSim. This pillar was then used as a benchmark to determine whether other pillars had failed. A residual strength of 20 MPa was assigned to all failed pillars.

Impala 10 shaft (Site 1)

These workings are located about 890 m below surface (Figure 11). Pillars 16 and 17 were observed to have burst some time after mining and sweeping had been completed in the stope (Figure 12).

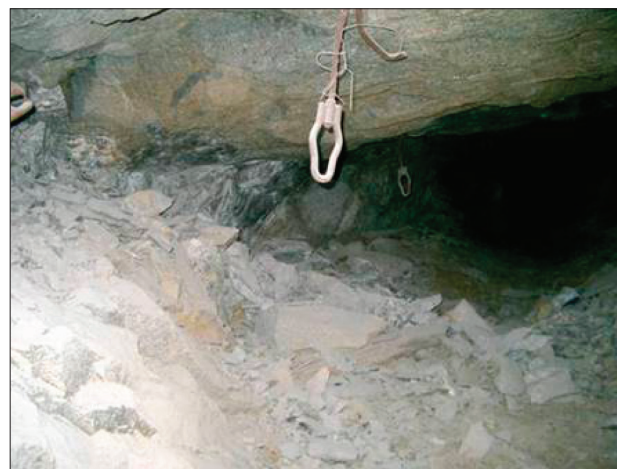


Figure 10—Pillar 14 and the fractured rock in the ASG after the burst

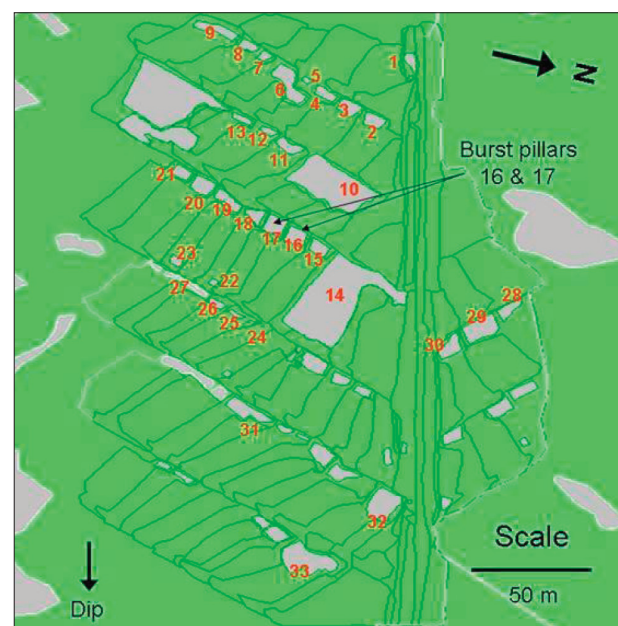


Figure 11—Plan showing the Impala 10 shaft investigation site (depth 890 m, dip 9°)

Merensky pillar strength formulae based on back-analysis of pillar failures



Figure 12—Up-dip side of Pillar 16

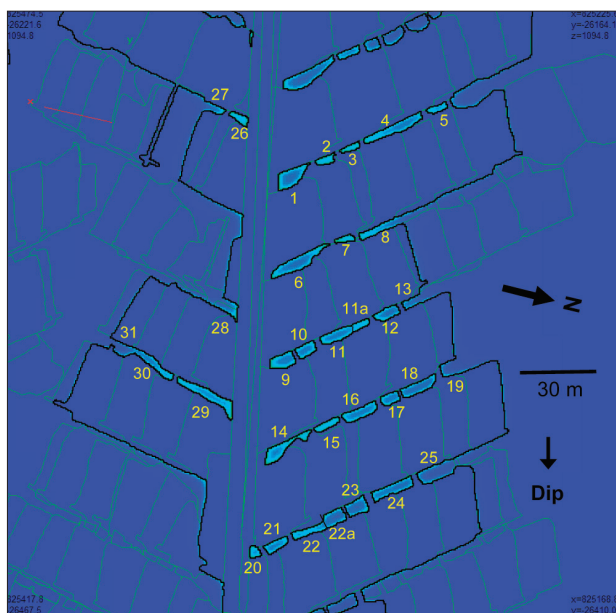


Figure 13—Plan showing the 2nd Impala 10 shaft investigation site (depth 1 100 m, dip 9°)

The pillars were assumed to be close to their load bearing capacity when the stope reached its limits and may have burst because of mining in the surrounding stopes or as a result of local seismicity. The pillar numbers shown in the plan were used in the analysis.

Impala 10 shaft (Site 2)

The stope was mined during the first half of 2005 using a breast configuration. The depth of workings and reef dip were about 1 100 m below surface and 9°, respectively. Pillars 11, 9 and 12 (Figure 13) burst on 25 March, 15 April and 17 April 2005, respectively. The face positions shown in Figure 13 did not change between the bursts.

The bursts took place during sweeping operations, when the rock left in the ASG was removed. This site provided strengths for large w/h ratio pillars. Figure 14 shows some of the broken fragments of rock in the siding on the up-dip side

of Pillar 9 after cleaning-up operations. Note the stress fractures in the hangingwall, indicating that the pillar was highly stressed at some stage.

Impala 10 shaft (Site 3)

The mining conditions were similar to Site 2. However, poor local ground conditions led to Pillar 24 (Figure 15) being cut to unusually large dimensions. The pillar burst at the mining configuration shown.

Maximum likelihood evaluation

Database description

The database consisted of 179 pillars, of which 109 represented stresses at some value below the peak strength, 8 were CC=3 pillars and 62 provided some stress higher than the strength. The majority of the pillar w_e/h_e ratios ranged

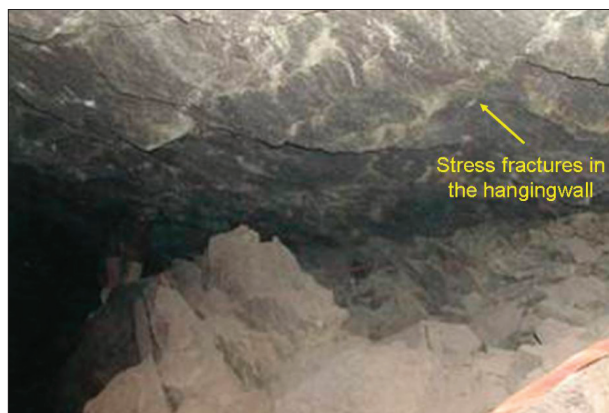


Figure 14—Up-dip side of Pillar 9

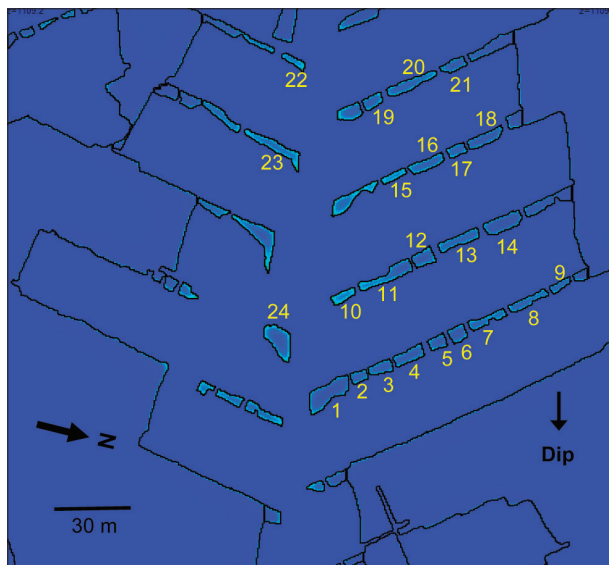


Figure 15—Plan showing the 3rd Impala 10 shaft investigation site (depth 1 100 m, dip 9°)

Merensky pillar strength formulae based on back-analysis of pillar failures

between 2 and 6, with the largest proportion being between 2.5 and 3.5 (Figure 16). Very little data was available below 1.5 or greater than 6.

The data-set included a wide range of pillar lengths (Figure 17) and widths (Figure 18) but all the heights fell into the limited range between 1.2 m and 2 m (Figure 19).

Two types of pillar strength formulae were back fitted, using the maximum likelihood evaluation:

- Linear formula¹² and
- Power formula⁹.

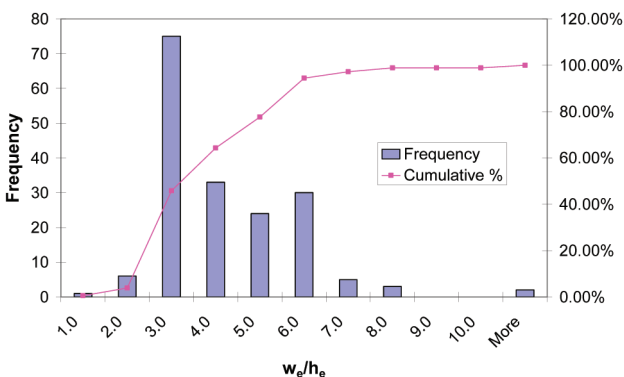


Figure 16—Distribution of pillar w_e/h_e in the database

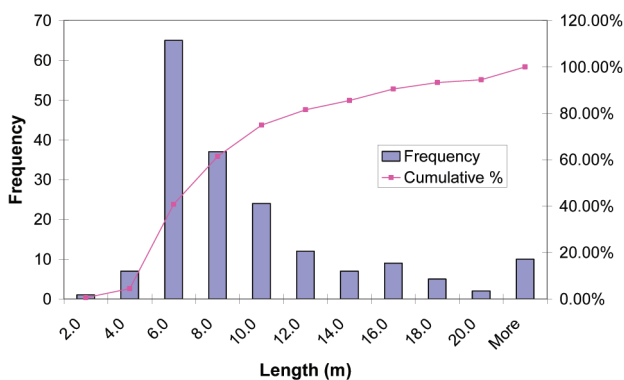


Figure 17—Distribution of pillar lengths in the database

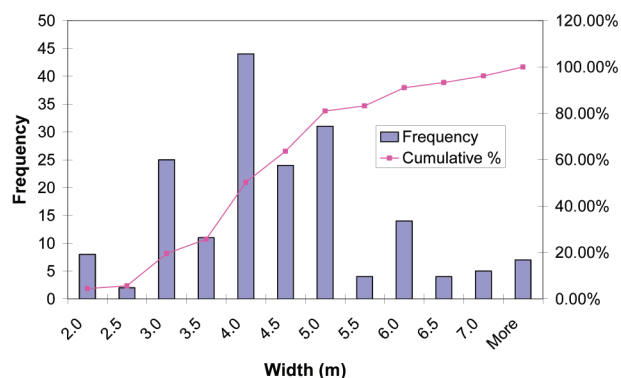


Figure 18—Distribution of pillar widths in the database

Linear formula

The linear equation, in its original form (Equation 6), assumes square pillars. Ryder *et al*⁴ modified the equation (Equation [7]) to obtain an explicit estimate of length (L) strengthening, partially based on expected strengthening under plane strain conditions¹³.

$$Strength = K_i \left[b + (1 - b) \frac{w}{h_e} \right] \quad [6]$$

$$Strength = K_i \left[\frac{1 + a}{1 + aw/L} \right] \left[b + (1 - b) \frac{w}{h_e} \right] \quad [7]$$

The back-fit values for Equation [7] are provided in Table I.

The *a* parameter predicts a 27% increase in the strength of a rib as opposed to a square pillar, which is similar to the strengthening effects suggested by Ryder and Ozbay¹³ and Roberts *et al*⁷ (~30%). The *b* parameter is similar to values obtained by Bieniawski and van Heerden¹² for large *in situ* South African coal specimens (*b*=0.64). The predicted *in situ* cube strength (*K_i*) appears slightly high as the laboratory UCS on a *w/h*=0.3 cylinder is only about 90 MPa. A comparison between the modelled and calculated APS values is shown in Figure 20. The Figure shows a good separation between failed and unfailed pillars, with a correspondingly low evaluated standard deviation *s*.

As an illustrative example of the use of Equation [7], a pillar with dimensions (L × *w/h_e*) of 6 m × 3 m/ 1.2 m, provides an estimated strength of 246 MPa.

The linear equation can also be used assuming *w_e* (perimeter rule)⁸ (Equation [3]) for rectangular pillars. Equation [6] can thus be rewritten as:

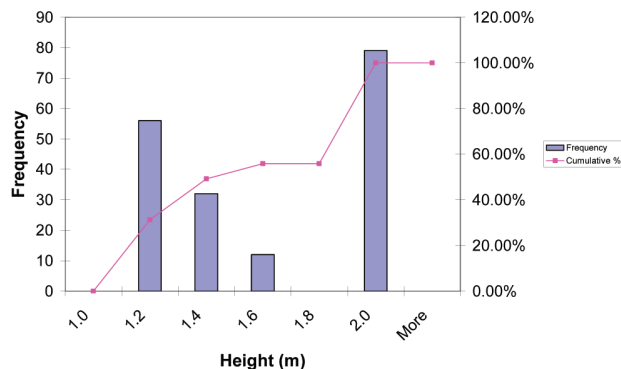


Figure 19—Distribution of pillar heights in the database

Table I Back fit values for Equation [7]	
Parameter	Value
<i>K_i</i> (<i>in situ</i> cube strength)	136 MPa
<i>a</i> (length parameter)	0.27
<i>b</i> (linear <i>w/h_e</i> parameter)	0.59
<i>s</i>	0.073

Merensky pillar strength formulae based on back-analysis of pillar failures

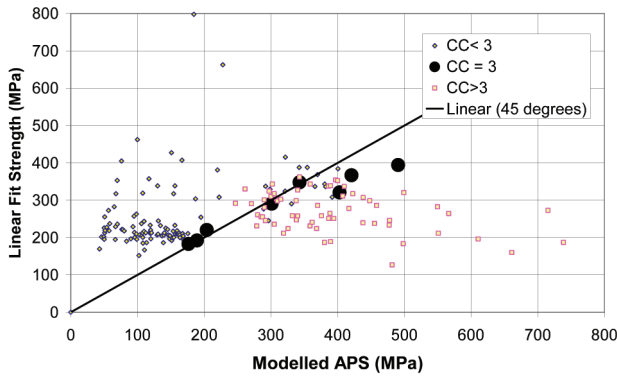


Figure 20—Backfit strengths, using the linear pillar strength formula (Equation [7])

Parameter	Value
K_i (<i>in situ</i> cube strength)	147 MPa
b (linear w/h_e parameter)	0.70
s	0.075

$$\text{Strength} = K_i \left[b + (1 - b) \frac{w_e}{h_e} \right] \quad [8]$$

Only two parameters are required in Equation 8 and the back-fit values are provided in Table II.

The calculated *in situ* cube strength (K_i) provided by the back-fit analysis on Equation [8] is higher than expected and the standard deviation s is also slightly higher than in Table I. However, the b value is similar to widely reported values (0.78) for materials including coal, norite and sandstone¹³. Figure 21 also shows a good separation between failed and unfailed pillars, but the strength prediction for the CC3 pillars is not as good as in Figure 20, particularly for higher w/h ratios.

Figure 22 compares the strengthening effects of the Ryder *et al.*⁴ and Wagner⁸ correction for length. The Wagner⁸ correction depends on w and h whereas the Ryder *et al.*⁴ adjustment is independent of these variables. Figure 22 represents the range of CC3 widths.

Power formula

Table III shows the results of the standard power formula backfit (Equation [9]). The length strengthening effects are implicit in the use of the perimeter-rule⁸ effective width w_e :

$$\text{Strength} = K w_e^\alpha h_e^\beta \quad [9]$$

These α and β values differ significantly from those back-fitted for the South African coal mines⁹ ($\alpha = 0.46$, $\beta = -0.66$) or for the Hedley and Grant¹⁴ formula ($\alpha = 0.50$, $\beta = -0.75$). The β value in Table III was determined from a relatively small range of heights (Figure 19) and may therefore be unreliable. The estimated strength using the power formula for a pillar with dimensions 6 m x 3 m ($w_e = 4$ m) and a

height of 1.2 m, is 231 MPa, slightly lower than that determined by the linear formula.

Figure 23 compares the modelled and calculated APS values. This also indicates a good separation between failed and unfailed pillars, but the CC3 pillars do not fit as well as in Figure 20. The standard deviation is also slightly higher than the analyses shown in Table I.

These initial investigations suggest a good correlation between calculated and actual strengths for both the linear and power formulae. However, the linear formula provides a slightly smaller standard deviation, and therefore better results for the whole database.

This linear relationship between strength and w/h is also supported if just the eight CC3 pillars are considered—Figure 24 and Figure 25.

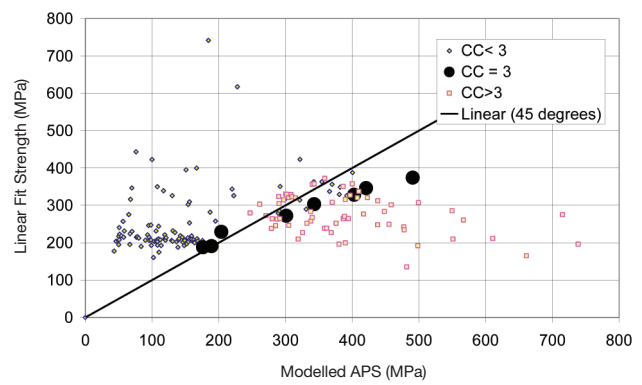


Figure 21—Back-fit strengths, using the linear pillar strength formula (Equation [8])

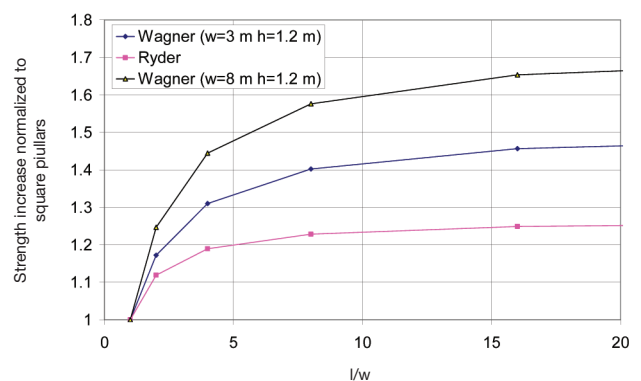


Figure 22—Comparison between the strengthening effects of pillar length for the Wagner⁵ (Equation [8]) and Ryder *et al.*¹ (Equation [7]) equations

Parameter	Value
K	86 MPa
α (effective width parameter)	0.76
β (effective height parameter)	-0.36
s	0.080

Merensky pillar strength formulae based on back-analysis of pillar failures

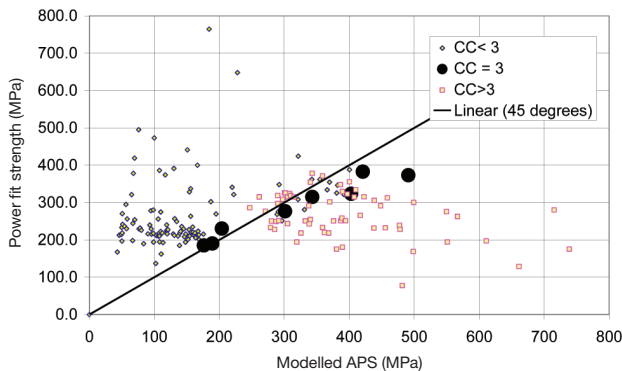


Figure 23—Back-fit strengths, using the power pillar-strength formula

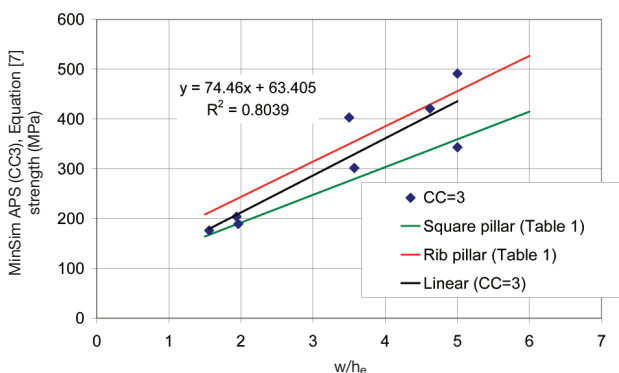


Figure 24—Linear regression of CC3 pillar strengths (MinSim) as a function of w/h_e , compared to strengths of square and rib pillars using Table I

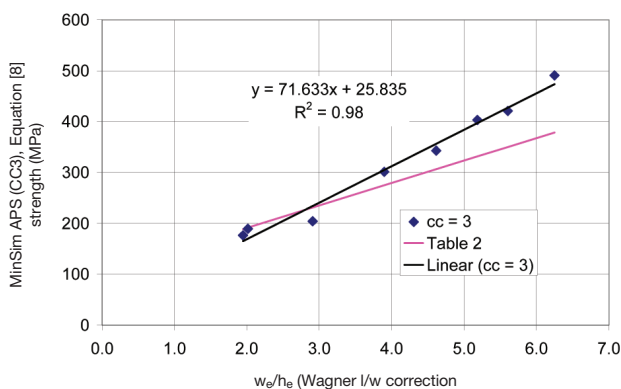


Figure 25—Linear regression of CC3 pillar strengths (MinSim) as a function of w_e/h_e (using the Wagner⁸ correction for length)

The results of the CC3 pillars show a similar relationship between pillar strength and w/h as the rest of the database. The regression shown in Figure 24 does not match the CC3 values as well as in Figure 25 because no correction has been made for the effect of pillar length on strength in Figure 24. Theoretically the CC3 data points should be located between the extremes of the square and rib pillars in Figure 24 and on the back analysed strength line in Figure 25. The slope of the CC3 regression line is, however, steeper than the slope of the back-analysed strength equations. These results suggest that

the database may be slightly underestimating the pillar strength at higher w/h . However, there were only eight CC3 pillars and their statistical relevance may be limited. It is interesting that the back-analyses suggest an approximately linear increase of strength even above w/h ratios of five. Squat-pillar theory¹⁴ suggests an exponential increase in strength at a w/h of greater than five. This theory, therefore, does not appear to apply to the pillars in the database; the reason, most probably, being that foundation-failure effects play a large role in determining the system strength of underground hard rock squat pillars. This is discussed in more detail in the following section.

The Wagner⁸ width correction for pillar length (Figure 25) provides a better correlation coefficient for linear regression analysis of the CC3 pillars than the Ryder *et al*⁴ evaluation in Figure 24, but only eight pillars were used in the assessment. In addition, the Wagner⁸ length strengthening effect for pillars with $w=3$ m and $h=1.2$ m, when applied to the linear equation with the constants in Table II (see Figure 22), provides similar results to Stravropoulou's¹⁶ findings, i.e. that a conventionally tested uniaxial specimen is 45% weaker than a sandstone tested under plane strain conditions. However, the Wagner⁸ correction is dependant on pillar w and h (see the curves in Figure 22 for 3 m and 8 m wide pillars), probably providing unrealistically high factors for the larger pillars in the database. The worse fit of the Ryder *et al*⁴ regression analysis (Figure 24) compared to the Wagner⁸ evaluation (Figure 25), and the larger influence of length on strength increase predicted by Stravropoulou¹⁶ suggests that the Ryder *et al*⁴ correction for length may be slightly conservative. The conservative nature of the Ryder *et al*⁴ correction for length, the smaller standard deviation shown in Table I and the better evaluation of larger pillars by Equation [7], suggests that this equation with the parameters in Table I is preferred over the Wagner⁸ length correction (Equation [8]) for the design of stable pillars.

The value for s in Table I was used to determine a range of safety factors. Safety factors have been plotted as a function of probability of stability in Figure 26, and may be used when designing stability pillars with similar geomechanical and geotechnical conditions to the pillars in the database. A safety factor of 1.7 will provide a probability of stability of 99.9%, on the basis of the limited data in the database.

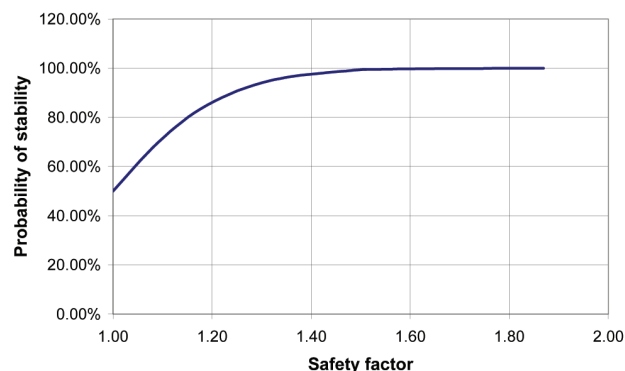


Figure 26—Safety factor for the Impala Merensky pillars as a function of probability of stability, based on the linear back-fit analysis (log $s=0.073$)

Merensky pillar strength formulae based on back-analysis of pillar failures

The database consisted of a mixture of pillars with and without sidings, and the siding depths and the heights of gullies also varied. The effect of these parameters on pillar strength was applied using unproven theory and needs to be investigated further.

FLAC strain softening analysis

Model description

FLAC¹⁷ was used to determine the response of a rib pillar system comprising the pillar itself and the immediate hanging- and footwalls. Of particular interest are the effects of w/h on pillar (system) strength. The results of laboratory tests, in combination with previous modelling work⁵ were initially used to select parameters that control the strength and the post-failure behaviour of the Merensky Reef pillars. Final parameters for the Mohr-Coulomb strength criterion were calibrated from the back-fit strength results of underground pillars.

As the triaxial laboratory test data showed a rapid build-up of the internal friction angle to a constant value, it was decided to represent the changes in material strength by a constant internal friction angle, combined with a linearly decreasing cohesive resistance. This allowed for a fairly simple constitutive model in which the maximum strength in the triaxial tests is determined by two constants: the internal friction angle and the initial cohesive strength. Post-failure behaviour is controlled by the loss of cohesion with increasing deformation.

Boundary conditions play an important role in the punching mechanism, as they affect horizontal confinement. In the models, the vertical boundaries are not allowed to move in a horizontal direction (thus simulating a fully replicated set of pillars). The presence of discontinuities such as bedding planes, faults and joints should also affect the punch resistance, but this has not been investigated in the present study.

While the numerical models provide insight into the failure mechanisms and allow quantification of the pillar system strength, it must be emphasized that these models always need to be calibrated against realistic data. Mesh density and rate of softening are important parameters in this respect and they cannot be arbitrarily selected. Table IV shows the parameters that have been used in the numerical model, as well as the parameters that are obtained from triaxial compression tests on pyroxenite and anorthosite (Figure 6 and Figure 7). The softening rate that has been used for the numerical models appears to be relatively large. Unfortunately, it was not possible to obtain realistic post-failure parameters from the laboratory tests, as failure localization obscured the data.

Results

The selected strength parameters for the Mohr-Coulomb strain softening model are a cohesive resistance of 20 MPa and an internal friction angle of 40°. This results in a UCS of 86 MPa, which is similar to the laboratory-determined UCS (Figure 6). The rate of cohesion softening (brittleness) has a major influence on the pillar strength, as can be discerned from Figure 27. Two extremes were selected: a relatively brittle material with a cohesion loss of 20 MPa over 25 millistrain (brittle model), and a relatively ductile material

with a cohesion loss of 20 MPa over 100 millistrain (ductile model). However, it was subsequently found that the mesh density, or the element size, also controls the 'effective brittleness'. The results displayed in Figure 27 are obtained from models with a high mesh density in which the pillar consisted of 48 square elements across the height of the pillar, which was kept constant in the 'constant height' models. The stope span was five times the pillar width (extraction ratio ~ 83%) and the model height was more than eight times the pillar width. The latter was varied in order to change the w/h ratio in the 'constant height' models, in which the number of elements across the width of the pillar increased proportionally. In order to investigate the possibility of this affecting punch resistance, another set of models, the 'constant width' models, was analysed. In these models, the height of the pillars was varied by using the same number of elements across the height (48), while changing the shape of the pillar elements from square to rectangular. All results are displayed in Figure 27 where it can be seen that the differences between the 'constant height'

Table IV

Material and model properties

	σ_3 (MPa)	C_0 (MPa)	ϕ_0	ϕ_{res}	ϵ_{pr} (mε)	ψ_0	ψ_{res}
A	2	15	55	50	< 0	-	-
	5	15	55	50	< 0	-	-
	10	15	55	40	< 0	-	-
P	2	16	52	50	0.75	-	-
	10	16	52	40	0.65	-	-
B		20	40	40	25	10	10
S		20	40	40	100	10	10

A = anorthosite lab.test,
P = pyroxenite lab.test,
B = brittle model,
S = ductile model,
 C_0 = cohesion,
 ϕ_0 = internal friction angle at peak load,
 ϕ_{res} = residual internal friction angle,
 ϵ_{pr} = residual plastic shear strain,
 ψ_0 = Dilation angle at peak load and
 ψ_{res} = residual dilation angle.

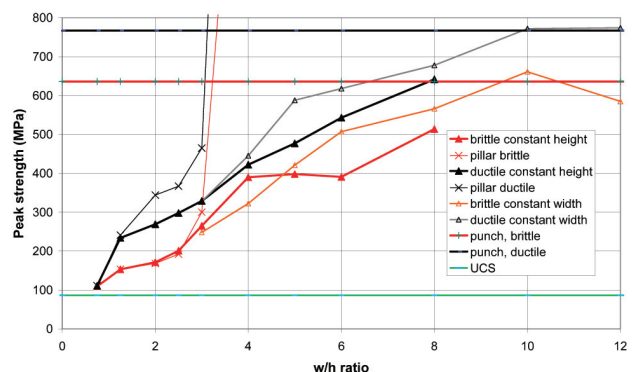


Figure 27—Effect of pillar w/h ratio for pillars that are allowed to punch, as well as for pillars that are surrounded by an infinitely strong rock mass; high density mesh and varying brittleness

Merensky pillar strength formulae based on back-analysis of pillar failures

and 'constant width' width models are relatively small. This is because an increase in mesh density does not have a substantial effect on punch resistance, once a certain mesh density is exceeded.

The graphs labelled 'pillar brittle' and 'pillar ductile' refer to models in which the hanging- and footwall material is not allowed to fail, so that punching is not possible and failure is concentrated in the pillar. Figure 27 also shows the pillar UCS, along with the ultimate punch resistance for these relatively brittle and ductile materials. These are labelled 'punch brittle' and 'punch ductile'.

As the graphs are based on a UCS of 86 MPa, a change in the value of the UCS would affect the values in the graphs proportionally.

While the softening rate (brittleness) and mesh density affect the effective pillar brittleness and consequently the effect of width-to-height ratio on strength, the mesh density also affects the punching potential of the pillar models. Models with a relatively high mesh density show a change in the mode of pillar failure once the pillar w/h ratio exceeds a certain value. At smaller w/h ratios, the pillars fail by progressively crushing from the edges towards the core, but in the wider pillars additional fracturing of the hanging- and/or footwall rock is initiated. Figure 27 shows that there is a disparity between the strengths of pillars with and without elastic foundations. This suggests that punching is initiated once the strength exceeds 250 MPa ($\sim 3 \times$ UCS).

If the hanging- and footwall material is relatively strong and failure is restricted to the pillar, the pillars become virtually indestructible at a width-to-height ratio in excess of 3.0 (the so-called 'squat' pillar effect). The graphs labelled 'pillar' in Figure 27 illustrate this effect. Laboratory experiments on hard rock pillar specimens, loaded between steel platens, have not demonstrated such an extreme exponential relationship between w/h ratio and strength. However, it should be emphasized that the boundary conditions in such laboratory experiments are not representative of in-stope pillars. The interface between the loading platen and the specimen provides limited friction¹⁸ while the draping effect of the stope is not represented. As a consequence, the laboratory specimens experience far less confinement than the *in situ* pillars and numerical modelling results are probably more representative of actual pillar behaviour.

A more realistic model includes the presence of the hanging- and/or footwall. In such a model the fracturing or damage can expand beyond the pillar itself. This 'punching' phenomenon becomes an important aspect of the failure mechanism of the pillar system, and effectively controls the pillar strength at larger width-to-height ratios. The graphs in Figure 27 suggest an approximately linear increase in pillar strength with an increasing w/h ratio. At relatively large w/h ratios, the punch resistance does, however, reach a maximum at the stress levels indicated in the figure. These levels indicate the ultimate punching resistance of infinitely stiff and strong pillars.

The fact that material brittleness has such a profound effect on system strength can be explained on the basis of the pillar failure process. Unlike in triaxial tests, where uniform stress conditions prevail prior to specimen failure, pillar failure initiates at the pillar edges and progresses gradually

towards the core of the pillar. Edge failure typically starts at a relatively low average pillar stress. Failure progression towards the pillar core is to a large extent controlled by the post-failure behaviour of the previously failed material near the pillar edge. A relatively ductile material would provide more resistance during its post-failure degradation, as it requires more deformation to become completely destroyed. Pillar failure progression will therefore be more restrained in the case of a more ductile material as compared to a more brittle material. This implies that an increasing pillar width-to-height ratio will be associated with a larger rate of strength increase in the case of a relatively ductile material, while the rate of strength increase will be minimal in the case of a very brittle material. This is consistent with the non-punching pillar results shown in Figure 27.

The relationship between pillar strength and width-to-height ratio is likewise influenced by mesh density. At higher densities, an increase in width-to-height ratio brings with it less of an increase of strength. This can be explained from the fact that an increased mesh density leads to an increase in effective brittleness. Fracture localization is enhanced in the case of a denser mesh, which implies that foundation fracturing is more likely to occur in a model with a fine mesh than in a model with a coarse mesh. However, foundation fracturing is not synonymous with foundation failure. Foundation failure is the final stage, in which vertical punching is accommodated by horizontal dilation. It appears that this dilation is induced at a lower resistance level when the element sizes are relatively large. In other words, a reduction in element size (and thus an increase in mesh density) would cause an increased punch resistance. This is in contrast to the effects of mesh density on the crushing of the pillar itself and on foundation fracturing. In order to obtain a representative material brittleness as well as a correct correlation between pillar failure and rock mass failure, the combination of mesh density and rate of cohesion softening needs to be calibrated properly. Most appropriate, obviously, would be the combination which results in the most accurate estimates of a wide range of pillar strengths. Figures 28 to 30 show the load-deformation characteristics and failure distributions for certain pillar geometries, mesh densities and cohesion softening rates.

It is of interest to note that the pillar with a w/h ratio of 2.0 is completely crushed, with limited failure in the footwall, while the pillar with a w/h ratio of 5.0 shows extensive

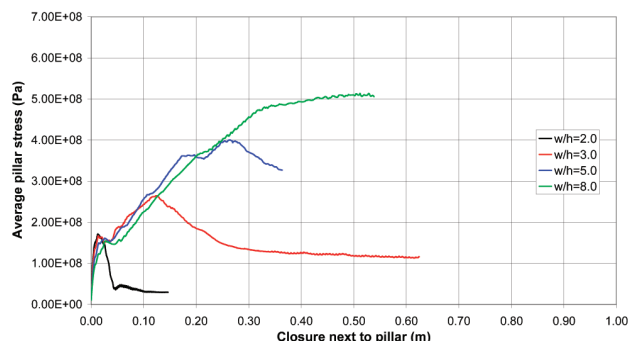


Figure 28—Load-deformation relationship; dense grid and most brittle material

Merensky pillar strength formulae based on back-analysis of pillar failures

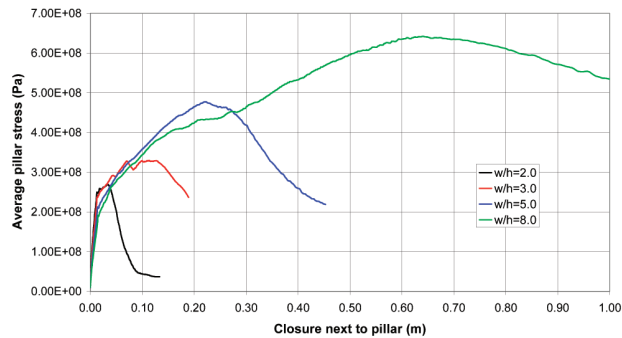


Figure 29—Load-deformation relationship; dense grid and least brittle material

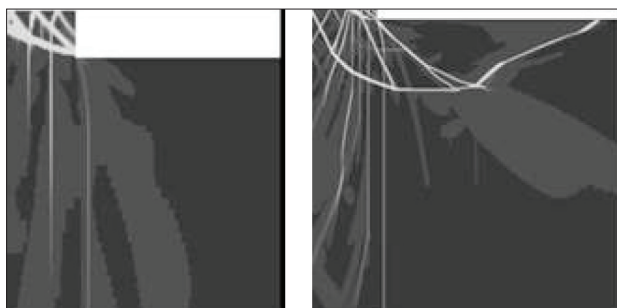


Figure 30—Failure distribution, using dense mesh and ductile material; $w/h = 2.0$ (left) and 5.0 (right) (double symmetry)

footwall failure combined with relatively large solid wedges in the core of the pillar. The typical ‘Prandtl wedge’¹⁹ formed in the footwall enables the footwall material to dilate into the stope, thus accommodating the actual pillar deformation and failure. Failure of a pillar system, which includes the adjacent footwall and/or hangingwall rock, involves in essence a combination of three mechanisms. First there is fracturing and crushing of the pillar itself, which often is reproduced under laboratory conditions with unrealistic boundary conditions. Then there is the fracturing into the surrounding material, the Herzian²⁰ crack and wedge formation. The third mechanism is the horizontal dilation of the foundation, which controls the ultimate resistance against punching. These latter two mechanisms have been investigated only to a very limited extent as far as brittle materials are concerned and references are therefore sparse (Cook *et al*²¹, Dede²², Özbay and Ryder²³, Wagner and Schümann²⁴). It is, however, clear that the failure of realistic pillar systems, with the probable exception of very slender pillars in hard rock, is to a large extent controlled by the fracture and failure processes in the foundation. These processes thus need to be included in any realistic analysis.

Discussion

The very small standard deviations in pillar strength estimated by the statistical back-analyses are evidence of a good quality database. An excellent correlation coefficient was obtained for the linear regression of the data relating pillar strength to w/h ratio for the CC3 pillars in Figure 24

and Figure 25. The analysis suggests that a linear formula is appropriate for strength analysis. Although the statistical relevance of only eight pillars may be limited, the back-analysis performed on the CC3 pillars also matches the strength parameters calibrated from the whole database very well (Figure 24 and Figure 25). The small value for s shown in Table I offers further evidence of a linear relationship between pillar strength and width-to-height ratio. The effect of length-to-width ratio has also been investigated in this study. As 90% of the pillars in the database have a length of less than 16 m, the range of w/l ratios is limited.

Nevertheless, when stresses calculated using the Ryder *et al*⁴ and Wagner⁸ length corrections are compared, the former such correction appears to be more realistic. This is especially true at greater pillar widths and lengths. The Wagner⁸ length correction appears to overestimate the pillar strength for wide and long pillars. We believe that Equation 7, with the back-fit parameters provided in Table I, provides the best estimate of pillar strength (at least for the range of w/h_c in the database) for the following reasons:

- The smaller standard deviation; and
- The reasonable (perhaps slightly underestimated) calculation of the effect of length on strength.

The numerical models (Figure 27) suggest that the w/h_c -strength relationship may not be linear at very high w/h_c ratios. It is suggested that the formula may be used on pillars with similar geotechnical and geomechanical characteristics to those of the pillar systems in the database. The effects of gullies adjacent to pillars and the depth of sidings have not been properly investigated and improved w/h ratio estimates may be possible when these factors are established. This would also enable a re-evaluation of the effects of pillar length on strength.

Figure 31 compares the strengths predicted by the linear formulae with those modelled in 2D by FLAC, by assuming infinitely long pillars. In this case, a good correlation has been obtained between underground data and the numerical results. Both indicate an approximately linear relationship between pillar strength and pillar w/h ratio. The numerical models demonstrate that the ultimate punch resistance is reached when the w/h ratio approaches 10. The results of the numerical models clearly show that pillars need to be viewed as a system that incorporates the immediate hanging- and footwall, as well as the pillar itself. With increasing w/h ratio,

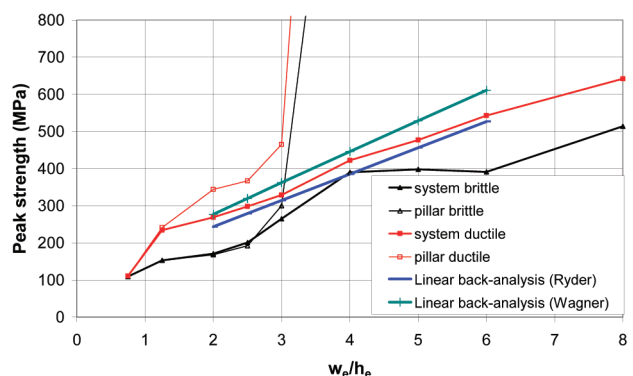


Figure 31—Comparison between the strength database and FLAC modelling results

Merensky pillar strength formulae based on back-analysis of pillar failures

failure is not contained solely within the pillar, but also expands into the hanging- and/or footwall. The so-called 'squat' effect is still present, but it no longer dominates the pillar system behaviour. Increasing pillar strength and pillar load results in increasing damage and failure in the hanging- and/or footwall.

The modelling results suggest that the pillar systems in the database compare very well with the 'ductile' model. This implies that footwall and/or hangingwall damage would have initiated at relatively low w/h ratio (~ 1.2), that is, for most of the pillars in the database. Under these conditions, pillar failure is always associated with footwall and/or hangingwall damage, and the pillar system's ability to carry load is reduced, as shown in Figure 28 and Figure 29. A further conclusion is that no benefit is gained by cutting pillars with a w/h ratio greater than about 10.

Conclusions

The database used in the paper to back analyse underground pillar strengths is shown to be high-quality. It included a wide range of widths w (2 m–7 m) and lengths L (4 m–20 m), though a lesser range of heights h_c (1.2 m–2 m). A convincing match was also obtained between FLAC modelling and the statistical analyses performed on the database. Both the database and the FLAC modelling suggest an approximately linear relationship between pillar strength and w/h ratio in areas where the pillars have geomechanical properties similar to those of the surrounding rock mass. The investigations suggest that Equation [7] with the constants in Table I best describe pillar strength for the pillars in this particular database. Analyses performed on the CC3 pillars indicate only that the constants in Table I may be slightly conservative and therefore safely applied to stable pillar design. Caution should be exercised when applying this formula and the calibrated constants to areas with different geotechnical and geomechanical properties.

The modelling demonstrates that pillar behaviour cannot be considered in isolation. Under conditions where the hangingwall and footwall have geomechanical properties similar to those of the pillar, foundation damage is inevitable, particularly for wider pillar systems. The pillars in the database followed the trends of the 'ductile' system in the model, indicating that damage would have initiated in the footwall and possibly the hangingwall for w/h ratios exceeding about 1.2. At higher w/h ratios, pillars may not necessarily fracture throughout, but the system fails with ensuing load loss. Thus, while the so-called squat effect persists, it does not dominate the system and a linear relationship is shown up to a w/h of about 10. No further strength increase was shown above a w/h of 10 and therefore no benefit is likely to be gained by cutting pillars larger than this.

Acknowledgements

PlatMine are acknowledged for facilitating the success of the project. In particular, the management and Rock Engineering Department of Impala Platinum Mine are thanked for their assistance.

References

- ROBERTS, M.K.C., GRAVE, D.M.H., JAGER, A.J. and KLOKOW, J. *Rock Mass Behaviour of the Merensky Reef at Northam Platinum Mine*. SARES, Johannesburg, 1997.
- COMRO. *MINSIM-D User's Manual*, Chamber of Mines of South Africa, Johannesburg, 1981.
- SPOTTISWOODE, S.M. and MILEV, A.M. A methodology and computer program for applying improved, inelastic ERR for the design of mine layouts on planar reefs. SIMRAC GAP722 Final Report. SIMRAC, Johannesburg, 2002. p.p 85.
- RYDER, J.A., WATSON, B.P. and KATAKA, M.O. Pillar strength back-analyses. *PlatMine* 1.2, Johannesburg, 2005.
- WATSON, B.P., KUIJPERS, J., NKWANA, M.M. and VAN ASWEGEN, L. The stress-strain behavior of in-stope pillars in the Bushveld Platinum deposits in South Africa. *J. South African Inst. Min. and Met.* vol. 107, 2007.
- ROBERTS, D.P., ROBERTS, M.K.C., JAGER, A.J. and COETZER, S. The determination of the residual strength of hard rock crush pillars with a width to height ratio of 2:1. *J. South African Inst. Min. and Met.* vol. 105, 2005. pp. 401–408.
- ROBERTS, D.P., CANBULAT, I. and RYDER, J.A. Design parameters for mine pillars: strength of pillars adjacent to gullies; design of stable pillars with w/h ratio greater than 6; optimum depth for crush pillars. SIMRAC GAP617 Final Report. SIMRAC, Johannesburg, 2002.
- WAGNER, H. Determination of the complete load-deformation characteristics of coal pillars. *Proceedings of 3rd International Congress on Rock Mechanics*, ISRM, Denver, vol. 2B, 1974. pp. 1076–1082.
- SALAMON, M.D.G. and MUNRO, A.H. A study of the strength of coal pillars. *J. South African Inst. Min. and Met.*, vol. 68, 1967.
- WAWERSIK, W.R. Experimental study of the fundamental mechanisms of rock failure. Thesis, U. of Minnesota, 1968.
- KOTZE, T.J. *A report on the collapse that took place in the 4 Shaft area of Bafokeng South*. Mine Internal Report no. G.R.M. 9/74, 1974.
- BIENIAWSKI, Z.T. and VAN HEERDEN, W.L. The significance of *in situ* tests on large rock specimens. *Int. J. Rock Mech. Min. Sci. & Geomech. Abstr.* vol. 12, 1975.
- RYDER, J.A. and OZBAY, M.U. A methodology for designing pillar layouts for shallow mining. *Int. Symp. on Static & Dyn. Conds. in Rock Eng.*, Swaziland, ISRM, 1990.
- HEDLEY, D.G.F. and GRANT, F. *Stope pillar design for the Elliot Lake uranium mines*. *Bull. Can. Inst. Min. Metall.*, 1972. pp. 65.
- MADDEN, B.J. *A re-assessment of coal-pillar design*. *J. South African Inst. Min. and Met.*, vol. 91, no. 1, 1991.
- STAVROPOULOU, V.G. Behaviour of a brittle sandstone in plane strain loading conditions. *Proc. 23rd U.S. Symp. on Rock Mechs.*, Berkeley, Cal. 1982.
- Itasca consulting group, inc. *Fast Lagrangian Analysis of Continua (FLAC)*, Vers. 3.2. Minneapolis Minnesota USA, 1993.
- YORK, G. Numerical modeling of the yielding of a stabilizing pillar/foundation system and a new design consideration for stabilizing pillar foundations. *J. South African Inst. Min. and Met.* vol. 98, 1998. pp. 281–293.
- PRANDTL, L. *Zeit. Angew. Math. Mech.* vol. T, no. 1, 1921. pp. 15–20.
- HERTZ, H. *On the contact of rigid solids and on hardness*, miscellaneous papers, Macmillan, London, 1896.
- COOK, N.G.W., HOOD, M. and TSAI, F. Observations of crack growth in hard rock loaded by an indenter. *Int. J. Rock Mech. Min. Sci. & Geomech. Abstr.*, vol. 21, no. 2, 1984. pp. 97–107.
- DEDE, T. Fracture onset and propagation in layered media. MSc dissertation, University of the Witwatersrand, Johannesburg, 1997.
- ÖZBAY, M.U. and RYDER, J.A. The effect of foundation damage on the performance of stabilizing pillars. *J.S. Afr. Inst. Min. Metall.*, vol. 90, no. 2, 1990. pp. 29–35.
- WAGNER, H. and SCHÜMANN, E.H.R. The stamp-load bearing strength of rock. An experimental and theoretical investigation. *Rock Mechanics*, vol. 3, 1971. pp. 185–207. ◆